Ultra-Wide-Bandgap Aluminum Gallium Nitride Devices for Radio-Frequency Applications

Robert J. Kaplar, Albert G. Baca, Brianna A. Klein, Joel R. Wendt, Stefan M. Lepkowski, Christopher D. Nordquist, Andrew M. Armstong, Andrew A. Allerman, Erica A. Douglas, Shahad Reza, and Jack D. Flicker
Sandia National Laboratories, Albuquerque, NM 87185; Email: rjkapla@sandia.gov

***Abstract*—The motivation for the use of ultra-wide-bandgap, Al-rich AlGaN for radio-frequency high electron mobility transistors is presented. An 8× increase in RF power is expected based on the anticipated 4× increase in breakdown electric field, 2× increase in channel sheet carrier density, and parity in electron saturation velocity for Al-rich AlGaN compared to GaN. Numerical simulations of HEMTs based on Al-rich AlGaN/AlGaN heterostructures indicate that a power density approaching 20 W/mm may be possible. Initial experimental results on an $Al_{0.85}Ga_{0.15}N/Al_{0.70}Ga_{0.30}N$ HEMT demonstrate the viability of the technology.**

Keywords—Ultra-Wide-Bandgap, Aluminum Gallium Nitride, High Electron Mobility Transistor, Radio Frequency

I. Introduction

Today's state-of-the-art technology in radio-frequency (RF) power amplifiers is capable of 5 W/mm using $Al_xGa_{1-x}N$/GaN HEMTs, with x typically in the range 0.25 – 0.30. The emerging material system based on Ultra-Wide-Bandgap (UWBG) Al-rich $Al_xGa_{1-x}N/Al_yGa_{1-y}N$ heterostructures with $0.7 \leq y < x \leq 1.0$ has the potential to greatly exceed the capabilities of today's AlGaN/GaN HEMTs, possibly achieving 20 W/mm power density. This projection stems from the expected 4× enhancement of critical electric field, 2× enhancement of sheet carrier density, and parity of electron saturation velocity for Al-rich AlGaN channel HEMTs relative to GaN-channel HEMTs. The anticipated increase in RF power density for Al-rich AlGaN-channel HEMTs is due in part to similarities to the existing AlGaN/GaN system, in part to theoretical analysis, and in part to existing data for long-channel Al-rich AlGaN-channel devices for power switching applications [1-5]. This work presents the theoretical basis for the use of Al-rich AlGaN for RF applications, and also presents initial experimental results for $Al_{0.85}Ga_{0.15}N/Al_{0.70}Ga_{0.30}N$ RF HEMTs.

II. Motivation for Al-Rich AlGaN RF Devices

To first order, the maximum RF power output from a transistor is given by the equation:

$$P_{max} = I_{max}V_{max}/8 \quad (1)$$

where I_{max} is the maximum RF current and V_{max} is the difference between the HEMT breakdown voltage and the knee voltage. Al-rich AlGaN-channel HEMTs have the potential in identically-sized devices to increase P_{max} relative to GaN-channel HEMTs due to a larger critical electric field E_c resulting from a larger bandgap E_g. The critical electric field of AlGaN has been observed to obey the power-law scaling:

$$E_c \sim E_g^{\,n} \quad (2)$$

with n in the range 2.5 – 2.7 [6], consistent with the prediction of Hudgins [7]. Current work is re-examining the reported experimental critical field values and their dependence on bandgap in more detail, and is also attempting to provide a theoretical explanation for the empirically observed power-law relationship between critical field and bandgap. A practical GaN-channel HEMT operates at an effective breakdown electric field of approximately 100 V/μm, roughly a quarter of the theoretical value. Assuming a similar 4× theoretical-to-achievable reduction factor for Al-rich AlGaN-channel HEMTs, it is expected that such a device could achieve a breakdown field of approximately 400 V/μm, or roughly 4× greater than that of a GaN-channel HEMT, for alloy compositions x in the 0.70 to 1.00 range. The significance of the 4× higher critical electric field for an Al-rich AlGaN-channel HEMT is that the sub-micron channel dimensions required for RF operation allow for biasing at a much larger voltage than is possible for a GaN-channel HEMT of the same physical size. Thus, a higher breakdown voltage for equivalent device dimensions (i.e. equivalent cutoff frequency f_T) should be achievable for AlGaN-channel HEMTs relative to GaN-channel HEMTs. Since power output in an RF power amplifier is proportional to the product of I_{max} and V_{max}, (Equation 1) the 4× higher critical electric field for AlGaN-channel HEMTs is expected to enable increases in power output deriving from higher voltage operation, as long as the requisite high current density can be achieved.

Regarding the current density, if the electric field is sufficiently high such that the velocity is saturated (as will be the case for RF operation), the current density is given by

$$J = qv_{sat}n_s \quad (3)$$

where q is the electron charge, v_{sat} is the electron saturation velocity, and n_s is the channel sheet carrier density. Based on Monte-Carlo simulations of electron saturation velocity in AlGaN, the saturation velocity is predicted to be of order 2×10^7 cm/s over the entire composition range, so that v_{sat} for Al-rich AlGaN is expected to be roughly equivalent to that of GaN [8]. Initial experimental measurements of $Al_{0.70}Ga_{0.30}N$ by our group have yielded $v_{sat} \approx 4\times10^6$ cm/s [9], and additional experiments are underway. From Equation (3), the other factor that determines current density, n_s, has already been observed by our group to exceed 2×10^{13} cm^{-2}, roughly double that typically observed for traditional AlGaN/GaN heterostructures. Indeed, there are good theoretical reasons to believe that achieving higher n_s in AlGaN-channel HEMTs than in GaN-channel HEMTs is plausible. One reason for this is the ability to tolerate a higher bandgap offset between channel and barrier, due to the higher strength of the Al-N bond compared to the Ga-N bond. Moreover, since the polarization charge increases

with increasing Al composition, at higher Al composition higher sheet carrier density is expected for comparable composition offset. Finally, since Al-rich heterostructures would likely be grown on AlN substrates, the barrier layer would be grown under compressive strain and could thus be grown thicker than the AlGaN barrier in an AlGaN/GaN HEMT. Due to these factors, a 2× improvement in n_s is expected for Al-rich heterostructures compared to conventional AlGaN/GaN heterostructures. Provided that the electric field is sufficiently high such that saturation velocity is achieved, this will result in a 2× increase in current density for an Al-rich AlGaN-channel device relative to a GaN-channel device, assuming parity in v_{sat}. All told, the expected 2× improvement in I_{max}, coupled with the 4× enhancement anticipated for V_{max}, predicts an 8× improvement in P_{max} for an Al-rich AlGaN-channel RF HEMT compared to a conventional GaN-channel RF HEMT.

Other aspects of the AlGaN material system may also lead to improved RF performance. The knee voltage is important because $V_{max} = V_{br} - V_{knee}$, so that V_{knee} impacts P_{max}. GaN-channel HEMTs have higher channel electron mobility than AlGaN-channel HEMTs do, and thus possess a smaller knee voltage. However, as a fraction of V_{max} this benefit is minimal at room temperature. Furthermore, RF devices typically operate at elevated temperatures. Since the low-field mobility of AlGaN is dominated by alloy scattering, it is not expected to be significantly less at elevated temperature than at room temperature [10], while the mobility of GaN will degrade considerably at high temperatures since it is dominated by phonon scattering. Thus, at high temperatures the knee voltage for a GaN-channel device is expected to be only slightly better than that of an AlGaN-channel device. Moreover, as a fraction of V_{max} the knee voltage of a GaN-channel device will likely be relatively worse than that of an AlGaN-channel device. These considerations suggest that AlGaN-channel devices not only offer potentially better power density than GaN-channel devices, but also superior Power-Added Efficiency (PAE). Finally, they may also offer improved linearity. Because RF linearity is lost at high power due to mobility-degradation-related channel resistance increases that result in a flattening of output power, AlGaN-channel devices are expected to show more robust linearity due to the insensitivity of mobility to temperature as discussed above.

III. Design Example

As an example, a HEMT consisting of an AlN barrier and an $Al_{0.70}Ga_{0.30}N$ channel was simulated [11]. A schematic drawing of the structure is shown in Figure 1. The barrier thickness underneath the gate, source, and drain metallizations was 10 nm, and the barrier thickness in the source-to-gate and gate-to-drain access regions was varied between 10 and 60 nm. The source-to-gate distance was 100 nm, the gate length was 100 nm, and the gate-to-drain distance was 500 nm. An $Al_{0.78}Ga_{0.22}N$ back-barrier was included in the design to reduce leakage current by improving carrier confinement, and the channel layer thickness between the barrier and the back-barrier was 150 nm.

Plots of the simulated drain current (I_d) and transconductance (G_m) vs. gate voltage are shown in Figure 2 for a drain-to-source voltage of 40 V and four values of the barrier thickness in the access regions. It is apparent that the thicker barrier results in not only a higher drain current, but also a higher, broader, and flatter transconductance curve, which are desirable attributes for higher power and greater linearity. However, the thicker barrier also results in higher drain leakage current in pinch-off due to the increased carrier density in the channel. For this reason, gain vs. frequency curves were simulated for the 40-nm-thick-barrier device. Mason's Unilateral Gain (MUG) vs. frequency curves for various gate voltages, derived from small-signal AC simulations, are shown in Figure 3. Biasing the device near the point of maximum transconductance (V_{gs} = 1 V) results in a gain of 34 dB at 30 GHz. Further, $f_T \approx 46$ GHz and $f_{max} \approx 230$ GHz are predicted, based on simulated $|h_{21}|$ vs. frequency curves (not shown).

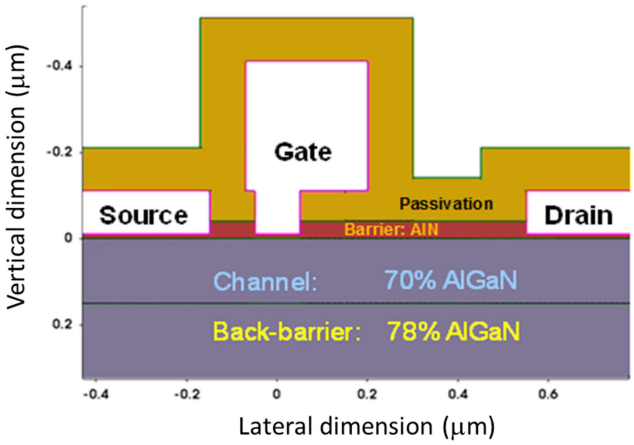

Figure 1. Schematic drawing of simulated $AlN/Al_{0.70}Ga_{0.30}N$ HEMT.

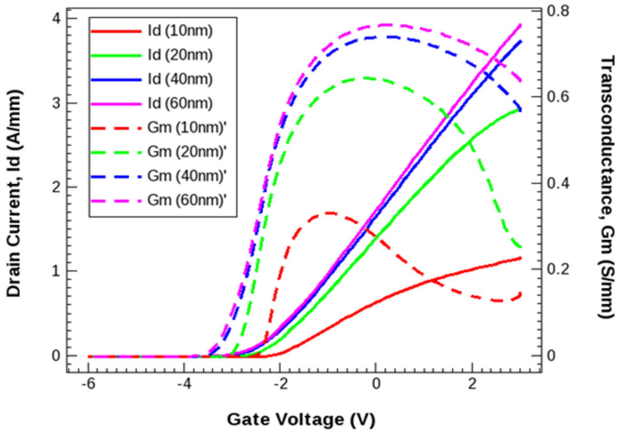

Figure 2. Simulated drain current and transconductance curves plotted vs. gate voltage for $AlN/Al_{0.70}Ga_{0.30}N$ HEMT for four access region barrier thicknesses. The drain voltage is 40 V.

The simulated drain current vs. drain voltage curves are shown in Figure 4. The bias current determines the gain, PAE, and third-order intercept point IP3. The best IP3 performance will be obtained at a DC bias (Q-point) near the maximum G_m

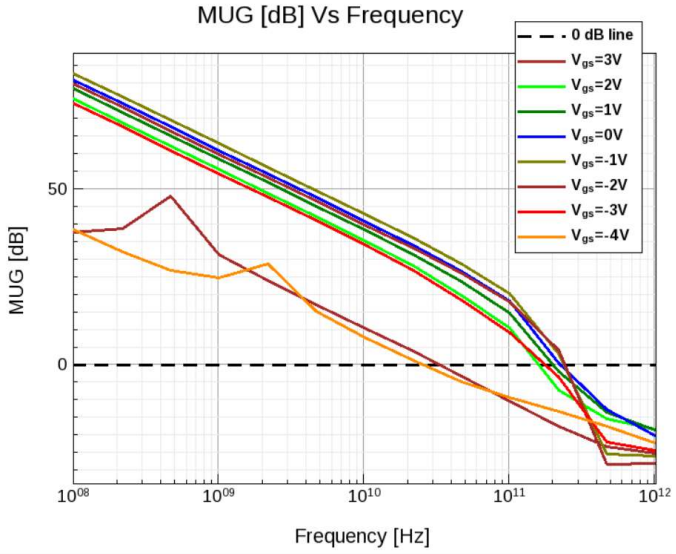

Figure 3. Simulated MUG for the 40-nm-thick barrier AlN/$Al_{0.70}Ga_{0.30}N$ device. The drain voltage is 40 V.

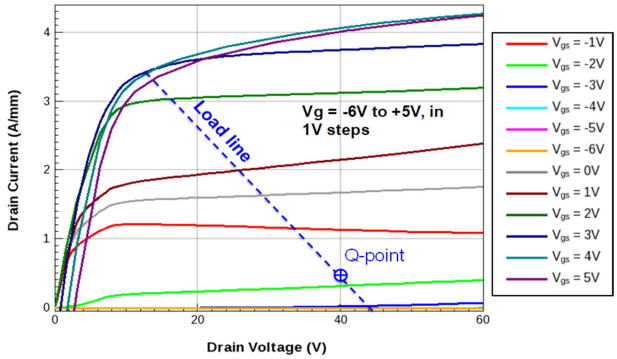

Figure 4. Drain current vs. drain voltage curves for the simulated device, with a resistive load-line superimposed.

point, which is at a drain current of ~1.8 A/mm (Figure 2). However, PAE will suffer because of the high DC bias current. Alternatively, a lower bias current will provide higher PAE, but IP3 performance will be degraded. To obtain first-order power and linearity performance, a Q-point of V_{gs} = -1.75 V, I_d = 0.37 A/mm was selected, even though this Q-point is not optimum for IP3.

Large-signal DC sweeps were performed using a load-line connecting the selected Q-point to the knee voltage at $V_{ds} \approx 10$ V, I_d = 3.4 A/mm, resulting in a load resistance of 9.1 Ω-mm (Figure 4). The V_{out} vs. V_{in} transfer curve was extracted by sweeping the gate input voltage (Figure 5a). From the extracted transfer curve, a MATLAB-based algorithm was used to calculate the output voltage and power waveforms for a 30 GHz sinusoidal input (Figure 5b). The input power was calculated from $V_{in}^2/Re[Z_{in}]$, where Z_{in} is the input impedance at the Q-point at 30 GHz. The output power at the fundamental (30 GHz) and the 3rd harmonic (90 GHz) was calculated from

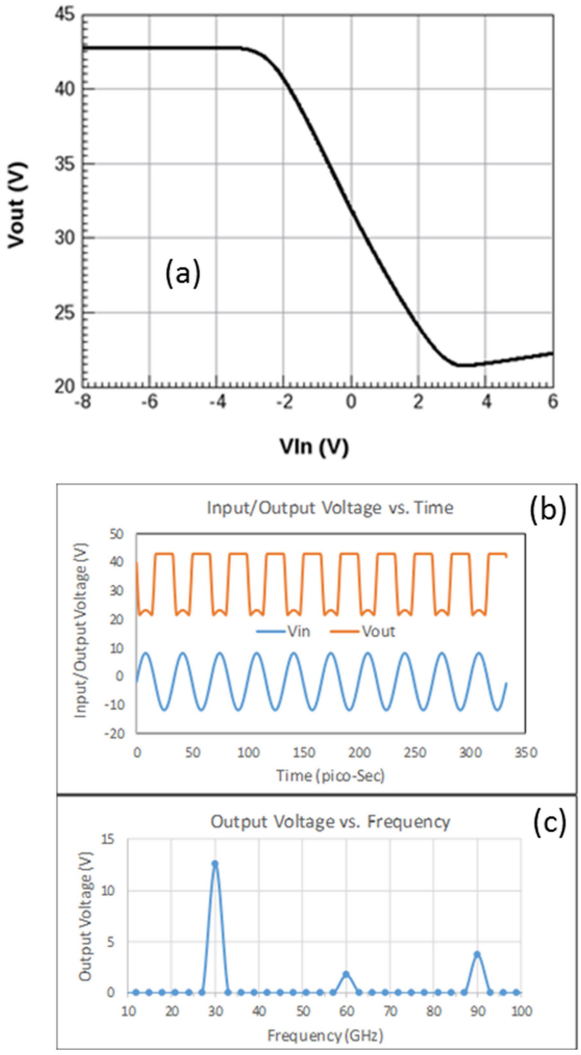

Figure 5. For simulated AlGaN-channel HEMT: (a) V_{out} vs. V_{in} transfer curve; (b) Input and output voltage waveforms; and (c) Frequency spectrum of the output voltage at 30 dBm input power.

the Fourier transform of the output voltage waveforms (Figure 5c). PAE was calculated from the input and output powers at 30 GHz and the DC power dissipation.

The calculated power performance for the AlGaN-channel HEMT is shown in Figure 6. For this design, a power density of 18 W/mm is achieved, substantially surpassing today's state-of-the-art ~5 W/mm. Several approaches exist that could plausibly increase the power density, for example increasing the barrier thickness, decreasing the Al mole fraction in the channel, and lowering the Al mole fraction in the back-barrier. All these approaches will result in increased charge and current density in the channel. A thicker barrier will also reduce the peak electric field within the device, likely resulting in not only a higher maximum voltage, but also in improved reliability.

IV. Initial Experimental Data

$Al_{0.85}Ga_{0.15}N/Al_{0.70}Ga_{0.30}N$ RF HEMTs were grown, fabricated, and characterized [12]. The growth was done by Metal-Organic Chemical Vapor Deposition (MOCVD) on sapphire substrates, and devices were processed in a manner similar to previous work on long-channel devices by our group [2,3]. The HEMTs were constructed using conventional rectangular geometry, a gate length of 80 nm, source-to-gate spacing of 0.5 µm, and gate-to-drain spacing of 2.0 µm. DC characterization of 50-µm-wide devices (Figure 7) yielded ~80 mA/mm at the bias condition V_{gs} = 5 V, V_{ds} = 10 V, with peak transconductance of 24 mS/mm near this bias point. Drain current increased to nearly 160 mA/mm when the device was biased at V_{gs} = 10 V, V_{ds} = 10 V.

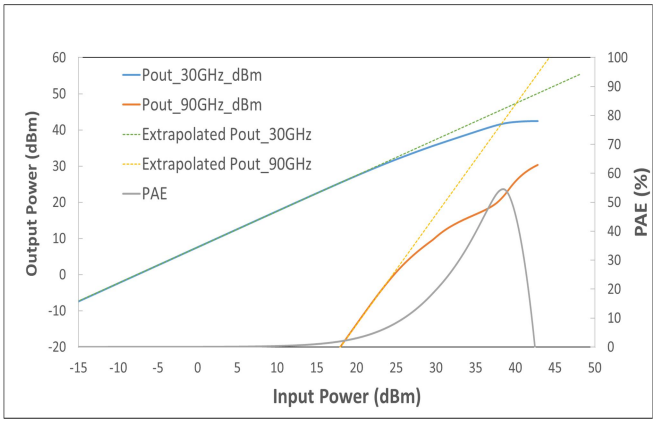

Figure 6. Power performance of the simulated AlGaN-channel HEMT.

Current and power gain vs. frequency plots derived from S-parameter measurements were used to determine f_T and f_{max} as a function of drain voltage. Results are plotted in Figure 8 as a function of drain voltage, at a gate voltage V_{gs} = 2.75 V. At the bias condition V_{gs} = 2.75 V, V_{ds} = 20 V, $f_T \approx$ 28.4 GHz and $f_{max} \approx$ 18.5 GHz. The reversal in order of frequency from what is expected (i.e. $f_T > f_{max}$ is observed, while typically $f_{max} > f_T$) may be due to gate resistance and/or drain conductance. Large-signal operation of a two-finger device at 3 GHz was performed at V_{gs} = 3.75 V, V_{ds} = 20 V to approximate class-A amplifier operation. Results for output power P_{out}, PAE, power gain G_p, and transducer gain G_t are plotted as a function of input power P_{in} in Figure 9. P_{out} = 15.8 dBm (0.38 W/mm) at the maximum PAE of 11%. These experimental results fall short of the simulated results, but are expected to improve considerably with improvements to the Ohmic contacts. These initial results demonstrate the viability of Al-rich AlGaN HEMT technology for RF applications, and compare favorably to other emerging UWBG technologies in this arena, such as Ga_2O_3 [13].

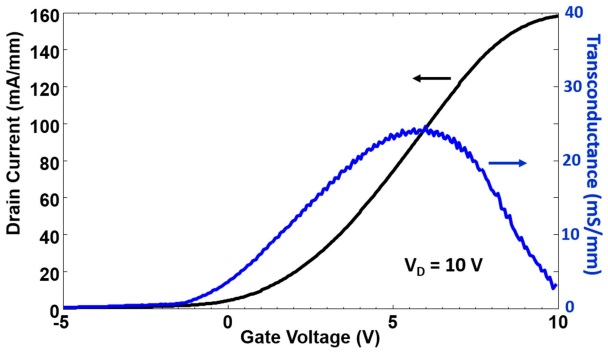

Figure 7. DC transfer characteristics for single-finger $Al_{0.85}Ga_{0.15}N/Al_{0.70}Ga_{0.30}N$ HEMT with 80 nm gate length and 50 µm gate width.

Acknowledgments

Sandia National Laboratories is a multi-program laboratory managed and operated by National Technology & Engineering Solutions of Sandia, LLC (NTESS), a wholly owned subsidiary of Honeywell Corporation, for the U.S. Department of Energy's National Nuclear Security Administration under contract DE-NA0003525. The views expressed in this article do not necessarily represent the views of the U.S. Department of Energy or the United States Government. A portion of this work was supported by the Laboratory Directed Research and Development (LDRD) program at Sandia.

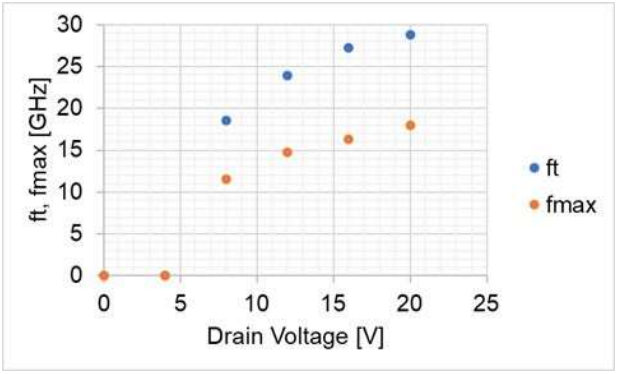

Figure 8. Cutoff frequency f_T and maximum oscillating frequency f_{max} for the HEMT of Figure 7 measured vs. drain voltage at V_{gs} = 2.75 V.

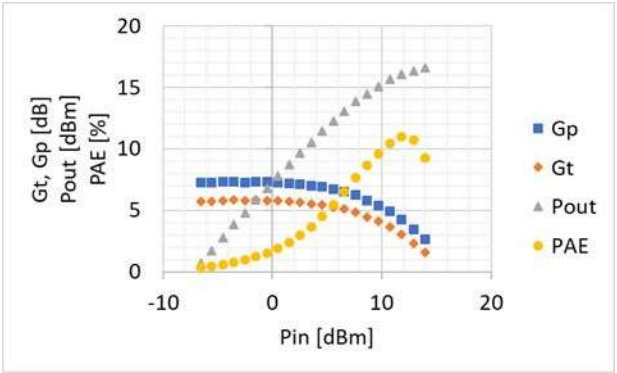

Figure 9. P_{out}, PAE, G_p, and G_t vs. P_{in} for two-finger $Al_{0.85}Ga_{0.15}N/Al_{0.70}Ga_{0.30}N$ HEMT with 80-nm-long gate.

REFERENCES

[1] T. Nanjo, M. Takeuchi, M. Suita, T. Oishi, Y. Abe, Y. Tokuda, and Y. Aoyagi, "Remarkable Breakdown Voltage Enhancement in AlGaN-Channel High Electron Mobility Transistors," *Appl. Phys. Lett.* **92**, 263502 (2008).

[2] A. G. Baca, A. M. Armstrong, A. A. Allerman, E. A. A. G. Baca, A. M. Armstrong, A. A. Allerman, E. A. Douglas, C. A. Sanchez, M. P. King, M. E. Coltrin, T. R. Fortune, and R. J. Kaplar, "An AlN/$Al_{0.85}Ga_{0.15}N$ High Electron Mobility Transistor," *Appl. Phys. Lett.* **109**, 033509 (2016).

[3] A. G. Baca, B. A. Klein, A. A. Allerman, A. M. Armstrong, E. A. Douglas, C. A. Stephenson, T. R. Fortune, and R. J. Kaplar, "$Al_{0.85}Ga_{0.15}N/Al_{0.70}Ga_{0.30}N$ High Electron Mobility Transistors with Schottky Gates and Large On/Off Curret Ratio over Temperature," *ECS J. Solid-State Sci. Tech* **6(12)**, Q161 (2017).

[4] S. Muhtadi, S. M. Hwang, A. Coleman, F. Asif, G. Simin, M. B. S. Chandrashekhar, and A. Khan, "High Electron Mobility Transistors with $Al_{0.65}Ga_{0.35}N$ Channel Layers on Thick AlN/Sapphire Templates," *IEEE Elec. Dev. Lett.* **38(7)**, 914 (2017).

[5] S. Bajaj, A. Allerman, A. Armstrong, T. Razzak, V. Talesara, W. Sun, S. H. Sohel, Y. Zhang, W. Lu, A. R. Arehart, F. Akyol, and S. Rajan, "High-Al-Content AlGaN Transistor with 0.5 A/mm Current Density and Lateral Breakdown Field Exceeding 3.6 MV/cm," *IEEE Elec. Dev. Lett.* **39(2)**, 256 (2018).

[6] A. Nishikawa, K. Kumakura, T. Akasada, and T. Makimoto, "High Critical Electric Field of AlGaN PiN Vertical Conduting Dioddes on n-SiC Substrates," *Appl. Phys. Lett.* **88**, 173508 (2006).

[7] J. L. Hudgins, G. S. Simin, E. Santi, and M. A. Khan, "An Assessment of Wide-Bandgap Semiconductors for Power Devices," *IEEE Trans. Power Elec.* **18(3)**, 907 (2003).

[8] M. Farahmand, C. Garetto, E. Bellotti, K. F. Brennan, M. Goano, E. Ghillino, G. Ghione, J. D. Albrecht, and P. P. Ruden, "Monte-Carlo Simulation of Electron Transport in the III-Nitride Wurtzite Phase Materials System: Binaries and Ternaries," *IEEE Trans. Elec. Dev.* **48(3)**, 535 (2001).

[9] B. A. Klein, A. G. Baca, S. M. Lepkowski, C. D. Nordquist, J. R. Wendt, A. A. Allerman, A. M. Armstrong, E. A. Douglas, V. M. Abate, and R. J. Kaplar, "Saturation Velocity Measurement of $Al_{0.7}Ga_{0.3}N$-Channel High Electron Mobility Transistors," submitted to *J. Elec. Mat.* (2019).

[10] M. E. Coltrin, A. G. Baca, and R. J. Kaplar, "Analysis of 2D Transport and Performance Characteristics for Lateral Power Devices Based On AlGaN Alloys," *ECS J. Solid-State Sci. Tech.* **6(11)**, S3114 (2017).

[11] S. Reza, B. A. Klein, A. G. Baca, A. M. Armstrong, A. A. Allerman, E. A Douglas, and R. J. Kaplar, "High-Frequency, High-Power Performance of AlGaN-Channel HEMTs: An RF Study," submitted to *Jap. J. Appl. Phys.* (2019).

[12] A. G. Baca, B. A. Klein, J. R. Wendt, S .M. Lepkowski, C. D. Nordquist, A. M. Armstrong, A. A. Allerman, E. A. Douglas, and R. J. Kaplar, "RF Performance of $Al_{0.85}Ga_{0.15}N/Al_{0.70}Ga_{0.30}N$ High Electron Mobility Transistors with 80 nm Gates," *IEEE Elec. Dev. Lett.* **40(1)**, 17 (2019).

[13] A. J. Green, K. D. Chabak, M. Baldini, N. Moser, R. Gilbert, R. C. Fitch Jr., G. Wagner, Z. Galazka, J. McCandless, A. Crespo, K. Leedy, and G. H. Jessen, "ß-Ga_2O_3 MOSFETs for Radio-Frequency Operation," *IEEE Elec. Dev. Lett.* **38(6)**, 790 (2017).